Minor Groove Orientation for the (1*S*,2*R*,3*S*,4*R*)-N^2-[1-(1,2,3,4-Tetrahydro-2,3,4-trihydroxybenz[*a*]anthracenyl)]-2′-deoxyguanosyl Adduct in the *N-ras* Codon 12 Sequence†

Hye-Young H. Kim, Amanda S. Wilkinson, Constance M. Harris, Thomas M. Harris, and Michael P. Stone*

Department of Chemistry, Center in Molecular Toxicology, Vanderbilt-Ingram Cancer Center, Vanderbilt University, Nashville, Tennessee 37235

Received July 9, 2002; Revised Manuscript Received November 26, 2002

ABSTRACT: The conformation of the *trans-anti*-(1*S*,2*R*,3*S*,4*R*)-N^2-[1-(1,2,3,4-tetrahydro-2,3,4-trihydroxybenz[*a*]anthracenyl)]-2′-deoxyguanosyl adduct in d($G^1G^2C^3A^4\underline{G^5X^6T^7}G^8G^9T^{10}G^{11}$)·d($C^{12}A^{13}C^{14}C^{15}A^{16}C^{17}C^{18}T^{19}G^{20}C^{21}C^{22}$), bearing codon 12 of the human *N-ras* protooncogene (underlined), was determined. This adduct had *S* stereochemistry at the benzylic carbon. Its occurrence in DNA is a consequence of trans opening by the deoxyguanosine amino group of (1*R*,2*S*,3*S*,4*R*)-1,2-epoxy-1,2,3,4-tetrahydrobenz[*a*]anthracenyl-3,4-diol. The resonance frequencies, relative to the unmodified DNA, of the X^6 H1′ and H6 protons were shifted downfield, whereas those of the C^{18} and T^{19} H1′, H2′, H2″, and H3′ deoxyribose protons were shifted upfield. The imino and amino resonances exhibited the expected sequential connectivities, suggesting no interruption of Watson−Crick pairing. A total of 426 interproton distances, including nine uniquely assigned BA−DNA distances, were used in the restrained molecular dynamics calculations. The refined structure showed that the benz[*a*]anthracene moiety bound in the minor groove, in the 5′-direction from the modified site. This was similar to the (+)-*trans-anti*-benzo[*a*]pyrene−N^2-dG adduct having *S* stereochemistry at the benzylic carbon [Cosman, M., De Los Santos, C., Fiala, R., Hingerty, B. E., Singh, S. B., Ibanez, V., Margulis, L. A., Live, D., Geacintov, N. E., Broyde, S., and Patel, D. J. (1992) *Proc. Natl. Acad. Sci. U.S.A. 89*, 1914−1918]. It differed from the (−)-*trans-anti*-benzo[*c*]phenanthrene−N^2-dG adduct having *S* stereochemistry at the benzylic carbon, which intercalated in the 5′-direction [Lin, C. H., Huang, X., Kolbanovskii, A., Hingerty, B. E., Amin, S., Broyde, S., Geacintov, N. E., and Patel, D. J. (2001) *J. Mol. Biol. 306*, 1059−1080]. The results provided insight into how PAH molecular topology modulates adduct structure in duplex DNA.

Benz[*a*]anthracene (BA),[1] a polycyclic aromatic hydrocarbon (PAH), is a component of coal tar, atmospheric pollution, automobile exhaust (*1*, *2*), and cigarette smoke (*3*). Its genotoxicity is generally recognized to result from stepwise oxidation by cytochromes P_{450} (*4*, *5*) to stereoisomeric bay region diol epoxides, which represent the proximate mutagenic and carcinogenic species. BA is less genotoxic than the well-known PAH benzo[*a*]pyrene. This has been attributed to less efficient enzymatic oxidation of BA in formation of the bay region diol epoxide (*6*). However, once formed, the BA bay region diol epoxides are mutagens in bacteria (*7*) and in Chinese hamster V79 cells (*8*). They are tumorigenic in mouse skin assays (*8*, *9*). The BA bay region diol epoxides react at nucleophilic sites on the DNA nucleobases, and particularly at the guanine N^2 (*7*, *10*−*16*), as well as adenine N^6 exocyclic amino groups (*17*−*19*). As with many PAH diol epoxides, the guanine N^2 adducts are of greater abundance than the corresponding adenine N^6 adducts (*20*, *21*).

The development of efficient routes to the site-specific synthesis of PAH-modified oligodeoxynucleotides (*22*−*27*) facilitated structural studies of a number of guanine N^2 PAH adducts (for a review, see ref *28*). Most of this work involved diastereomeric adducts arising from the *anti*-benzo[*a*]pyrene diol epoxides (*29*−*35*). The first high-resolution PAH−oligodeoxynucleotide structures were obtained for the (+)-*trans-anti*-[BP]−N^2-dG and (−)-*trans-anti*-[BP]−N^2-dG adducts (*29*, *30*). These had the ligand oriented in the minor groove, with the stereochemistry of the benzylic carbon

† This work was supported by NIH Grant ES-05355. Funding for the NMR spectrometers was supplied by Vanderbilt University, by NIH Grant RR-05805, and by the Vanderbilt Center in Molecular Toxicology (ES-00267). The Vanderbilt-Ingram Cancer Center is supported by NIH Grant CA-68485.

* To whom correspondence should be addressed. Phone: (615) 322-2589. Fax: (615) 322−7591. E-mail: stone@toxicology.mc.vanderbilt.edu.

[1] Abbreviations: BA, benz[*a*]anthracene; BcPh, benzo[*c*]phenanthrene; BP, benzo[*a*]pyrene; DE2, bay region diol epoxide 2 of benz[*a*]anthracene, (±)-4β,3α-dihydroxy-2α,1α-epoxy-1,2,3,4-tetrahydrobenz[*a*]anthracene; DQF-COSY, double-quantum-filtered correlation spectroscopy; eCOSY, exclusive correlation spectroscopy; EDTA, ethylenediaminetetraacetic acid; HPLC, high-pressure liquid chromatography; 5MC, 5-methylchrysene; NOE, nuclear Overhauser enhancement; NOESY, two-dimensional NOE spectroscopy; PAH, polycyclic aromatic hydrocarbon; PEM, potential energy minimization; rmsd, root-mean-square deviation; SO, styrene oxide; TOCSY, total correlation spectroscopy; TPPI, time-proportional phase incrementation; rMD, restrained molecular dynamics; 1D, one-dimensional; 2D, two-dimensional. A right superscript refers to the numerical position in the sequence starting from the 5′-terminus of chain A and proceeding to the 3′-terminus of chain A, and then from the 5′-terminus of chain B to the 3′-terminus of chain B.

10.1021/bi020462k CCC: $25.00
Published on Web 02/05/2003

Chart 1: (A) BA SRSR (12,2) Oligodeoxynucleotide Sequence and (B) (1*S*,2*R*,3*S*,4*R*)-N^2-[1-(1,2,3,4-Tetrahydrobenz[*a*]anthracenyl)]-2′-deoxyguanosyl Adduct and Designations of the Benz[*a*]anthracene Protons

A

ras codons

11 12 13

5′-G¹ |G² C³ A⁴ |G⁵ X⁶ T⁷ |G⁸ G⁹ T¹⁰ |G¹¹-3′

3′-C²² |C²¹G²⁰T¹⁹ |C¹⁸C¹⁷A¹⁶ |C¹⁵C¹⁴A¹³ |C¹²-5′

B

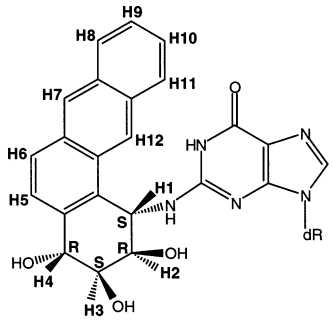

determining its orientation. The (+)-*trans-anti* diastereomer was oriented in the 5′-direction, whereas the (−)-*trans-anti* diastereomer was oriented in the 3′-direction (*30*). These two diastereomers had 10*S* and 10*R* designations at benzylic C10, respectively. Of other guanine N^2 *trans-anti* PAH adducts, the 5-methylchrysene (−)-*trans-anti*-[5MC]−N^2-dG diastereomer oriented in the 3′-direction in the minor groove (*36*). This adduct had the 4*R* designation at the benzylic carbon. The (+)-*trans-anti*-[5MC]−N^2-dG adduct (4*S* designation at the benzylic carbon) was disordered, precluding structural elucidation (*28*). The benzo[*c*]phenanthrene (−)-*trans-anti*-[BcPh]−N^2-dG adduct having *S* stereochemistry at the benzylic position intercalated in the 5′-direction (*37*). PAH *anti*-diol epoxides can also open with *cis* stereochemistry at the site of adduction. The (+)-*cis-anti*-[BP]−N^2-dG and (−)-*cis-anti*-[BP]−dG diastereomers exhibited base-displaced intercalation, with the BP moiety centered between the two flanking base pairs. The displacement of the modified deoxyguanosine toward the minor or major groove was determined by the stereochemistry at benzylic C10 (*31*, *38*).

The oligodeoxynucleotide 5′-d(GGCAGGTGGTG)-3′•5′-d(CACCACCTGCC)-3′, containing the codon 12 sequence (underlined) of the human *N-ras* protooncogene (*39*), was of interest because mutations in codon 12 are frequently found in tumor cells (*40*). Also, the *anti* isomers of BP diol epoxides are mutagenic in codons 12 and 61 of the human *c-Ha-ras1* protooncogene (*41*). Previously, this oligodeoxynucleotide was used to examine the styrene oxide *R*- and *S*-[SO]−N^2-dG adducts. As observed for the *trans-anti*-[PAH]−N^2-dG adducts, the *R*-[SO]−N^2-dG adduct was oriented in the 3′-direction, while the *S*-[SO]−N^2-dG adduct was oriented in the 5′-direction (*42*, *43*).

The work presented here describes the solution structure of the (1*S*,2*R*,3*S*,4*R*)-N^2-[1-(1,2,3,4-tetrahydrobenz[*a*]anthracenyl)]-2′-deoxyguanosyl adduct incorporated into 5′-d(GGCAGXTGGTG)-3′•5′-d(CACCACCTGCC)-3′, where X is the adducted guanine located at position 2 of codon 12. This is named the BA SRSR (12,2) adduct (Chart 1) (*26*). Structural refinement demonstrates that the anthracenyl moiety orients in the minor groove in the 5′-direction from the modified guanine. This is similar to the (+)-*trans-anti*-[BP]−N^2-dG adduct having the corresponding stereochemistry (*29*, *30*). It differs from the (−)-*trans-anti*-[BcPh]−N^2-dG adduct having the corresponding stereochemistry (1*S* at the benzylic carbon) which intercalates (*37*). The results address the role of the PAH molecular topology in determining the adduct structure at guanine N^2, and may have implications with regard to the biological processing of these lesions.

MATERIALS AND METHODS

Materials. The oligodeoxynucleotide 5′-d(GGCAGXTGGTG)-3′ (Chart 1) was synthesized by reacting the (±)-aminotriol derived from (±)-4β,3α-dihydroxy-2α,1α-epoxy-1,2,3,4-tetrahydrobenz[*a*]anthracene [(±)-DE2] with an oligodeoxynucleotide containing 2-triflate O^6-paranitrophenethyl deoxyinosine at position X^6 (*26*, *44*). The oligodeoxynucleotide 5′-d(CACCACCTGCC)-3′ was purchased from the Midland Certified Reagent Co. (Midland, TX). The BA SRSR (12,2) oligodeoxynucleotide was purified from the reaction mixture by HPLC using a phenyl-hexyl semi-preparative column (25 cm × 4.7 cm, Phenomenex) equilibrated with 10 mM triethylammonium acetate (pH 7.0). The oligodeoxynucleotide was eluted with a methanol gradient (0 to 30% methanol over the course of 8 min, 31.6% methanol for 34 min, and 90% methanol for 2 min). The diastereomer that eluted at 37 min was identified as the BA SRSR (12,2) adduct by circular dichroism, enzymatic digestion, and mass spectrometry. The BA SRSR (12,2) oligodeoxynucleotide was lyophilized and desalted on a Sephadex G-25 column (70 cm × 1.5 cm) (Amersham-Pharmacia, Inc., Piscataway, NJ).

The modified and complementary oligodeoxynucleotides were annealed at a 1:1.2 modified strand:complementary strand molar ratio in a buffer containing 0.1 M NaCl, 10 mM sodium phosphate, and 50 μM Na_2EDTA (pH 7.0). The mixture was heated to 90 °C for 3 min and cooled to room temperature. The duplex was eluted from DNA grade Bio-Gel hydroxylapatite (Bio-Rad Laboratories, Hercules, CA) (15 cm × 3.0 cm) with a sodium phosphate gradient (from 10 to 200 mM over the course of 90 min; pH 7.0). The duplex was desalted on a Sephadex G-25 column (70 cm × 1.5 cm). It was lyophilized and resuspended in 0.25 mL of NMR buffer [0.1 M NaCl, 10 mM sodium phosphate, and 50 μM Na_2EDTA (pH 7.0)]. The sample used for examining nonexchangeable protons was dissolved in 99.996% D_2O. The sample used for the examination of the exchangeable protons was dissolved in a 9:1 H_2O/D_2O mixture. In both instances, the duplex concentration was 1.7 mM.

NMR. Experiments were performed at ^1H frequencies of 600.13 and 800.23 MHz. The watergate pulse sequence suppressed the water signal (*45*−*47*). The spectra were recorded at 5 and 25 °C with a mixing time of 250 ms. The phase-sensitive NOESY spectra used for the assignment of nonexchangeable proton resonances were recorded at 25 °C with a mixing time of 200 ms using TPPI phase cycling, with a 2 s relaxation delay. Data were recorded with 2048 real points in the d_1 dimension and 1024 real points in the d_2 dimension. The data in the d_1 dimension were zero-filled to give a matrix of 2K × 2K real points. A skewed sinebell-square apodization function with a 70° phase shift was used

in both dimensions. TOCSY spectra with a 10 kHz spin-lock field were recorded with a mixing time of 150 ms using the MLEV17 (*48*−*50*) sequence. Data were transferred to Octane workstations (Silicon Graphics, Inc., Mountain View, CA) and processed using FELIX (version 97.0, Accelrys, Inc., San Diego, CA).

Distance Restraints. NOESY spectra were acquired at mixing times of 100, 150, and 200 ms. Footprints were drawn around cross-peaks for the spectrum measured with a mixing time of 200 ms. Cross-peak intensities were determined by volume integration. The same set of footprints was applied to spectra measured at other mixing times. The intensities were combined as necessary with intensities generated from complete relaxation matrix analysis of model B-form (IniB) and A-form (IniA) structures (*51*) to generate hybrid intensity matrices (*52*), from which distances were calculated using MARDIGRAS (version 3.0) (*53*, *54*). The molecular motion was assumed to be isotropic. Trial calculations were run using correlation times of 2, 3, and 4 ns. The noise in peak volumes was set at an absolute value of one-half the volume of the smallest peak measured in each spectrum. The algorithm RANDMARDI (*55*) generated error bounds in calculated distances consistent with the experimental noise level in the spectra and the relative error assessed in volume measurements. RANDMARDI carried out 50 calculations of each set of spectral data, randomizing the value of each measured volume within the limits specified by the input noise level and the relative volume errors at each iteration. This yielded three sets of calculated distances from each NOESY experiment, which were averaged. The standard deviation in each distance was used as the upper and lower distance bound in subsequent calculations. The distance restraints for subsequent rMD and PEM calculations were divided into five classes on the basis of confidence (*56*).

Deoxyribose pseudorotation restraints were determined from DQF-COSY data using sums of ^{3}J ^{1}H coupling constants (*57*). These were fit to curves relating coupling constants to pseudorotation, sugar pucker amplitude, and the percentage of S-type sugar conformation. Heteronuclear ^{1}H−^{31}P correlation spectra (*58*) using selective IBURP-shaped pulses (*59*) were used to obtain ^{31}P−H3′ couplings. Dihedral restraints for the ϵ and ζ sugar−phosphate backbone angles were derived from the ^{31}P−^{1}H ^{3}J data (*58*). The Karplus relationship was used to determine the phosphodiester torsion angle ϵ (C4′−C3′−O3′−P) (*60*), related to the H3′−C3′−O3′−^{31}P torsion angle by a 120° shift. The phosphodiester torsion angle ζ (C3′−O3′−P−O5′) was calculated from the correlation between ϵ and ζ in B-DNA (*61*).

Restrained Molecular Dynamics. Restrained molecular dynamics (rMD) calculations and potential energy minimization (PEM) calculations were carried out using X-PLOR (*62*) (version 3.85). The partial charges assigned to the BA moiety are shown in Figure S1 of the Supporting Information. The CHARMM force field (*63*, *64*) contributed the terms for bonds, bond angles, torsion angles, tetrahedral and planar geometry, hydrogen bonding, and nonbonding interactions, including van der Waals and electrostatic forces for the empirical portion of the energy function (*65*). The electrostatic term used the Coulomb function based on a reduced charge set of partial charges and a distance-dependent dielectric constant of 4.0, to mimic solvent screening of charge. The van der Waals term was approximated using the Lennard-Jones potential energy function. The effective energy function was comprised of two terms describing distance and dihedral restraints, both of which were in the form of standard square well potentials (*66*, *67*). Bond lengths involving hydrogens were fixed with the SHAKE algorithm (*68*) during calculations. The nonbonded pair list was updated if any atom moved more than 0.5 Å. The cutoff radius for nonbonded interactions was 11 Å. Calculations were run in vacuo, without explicit counterions.

Calculations were initiated by coupling the system to a heating bath with a target temperature of 1000 K. Force constants of 10 kcal mol^{-1} Å^{-2} were used for empirical hydrogen bonding, 20 kcal mol^{-1} Å^{-2} for torsion angle restraints, and 50, 45, 40, 35, and 30 kcal mol^{-1} Å^{-2} for the five classes of NOE restraints. The target temperature was reached in 5 ps and was maintained for 15 ps. The molecules were cooled to 300 K over 5 ps and maintained at that temperature for 15 ps of equilibrium dynamics. The force constants for the five classes of NOE restraints were scaled up for 3.5 ps during the heating period to 150, 130, 100, 100, and 100 kcal mol^{-1} Å^{-2} in the order of confidence factor. These weights were maintained during the reminder of the heating period and for the first 5 ps of the equilibrium dynamics period. They were then scaled down to 50, 45, 40, 35, and 30 kcal mol^{-1} Å^{-2} in the order of confidence factor. The torsion angle and base pair distance force constants were scaled up to 100 kcal mol^{-1} Å^{-2} during the same period as for the NOE restraints. They were scaled back to 20 and 10 kcal mol^{-1} Å^{-2}, also at the same time as the NOE restraints. Coordinate sets were archived every 0.1 ps, and 49 structures from the last 10 ps were averaged. These average rMD structures were subjected to conjugate gradient energy minimization, for 1100 iterations, to obtain the final structures.

Final structures were analyzed using X-PLOR to measure the rmsd between an average structure and the converged structures. Back calculation of theoretical NMR intensities from the emergent structures was performed using CORMA (version 4.0) (*52*). Helicoidal analysis of the structures was accomplished using 3DNA (http://rutchem.rutgers.edu/~xiangjun/3DNA/) (*69*).

RESULTS

^{1}H Resonance Assignments

Nonexchangeable Protons. An expanded NOE spectrum showing the pattern of sequential connectivity between the aromatic and anomeric protons is displayed in Figure 1. The sequential assignments for both strands of the oligodeoxynucleotide duplex were obtained without interruptions (*70*, *71*). The notable features observed in this region of the spectrum for the modified strand were downfield chemical shifts for X^{6} H8 and X^{6} H1′, relative to those of the unmodified oligomer (*39*). In the complementary strand, upfield chemical shifts were observed for C^{18} H1′ and T^{19} H1′ sugar protons. The C^{18} H1′ resonance was observed at δ 4.23 ppm, and the T^{19} H1′ resonance was observed at δ 4.68 ppm. These upfield shifts were compared with similar upfield shifts for the C^{18} H2′ and H2″ and T^{19} H2′ and H2″ protons, the assignments for which were obtained from a combination of TOCSY, DQF-COSY, and eCOSY (*72*) spectra. For C^{18}, H2′ was observed at δ 1.29 ppm and H2″

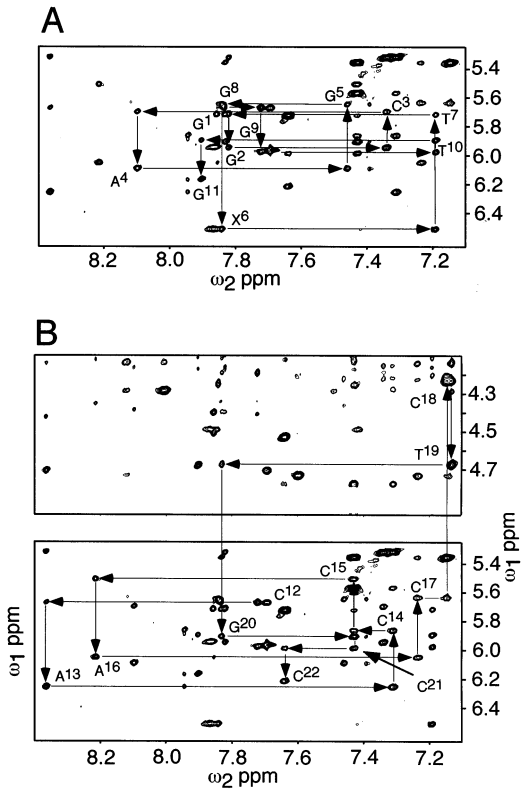

FIGURE 1: Expanded plot from a 800.23 MHz NOESY spectrum at a mixing time of 200 ms showing sequential NOE connectivities from the aromatic to H1′ protons. (A) Sequential NOE connectivities for nucleotides G^1−G^{11}. (B) Sequential NOE connectivities for nucleotides G^{12}−G^{22}.

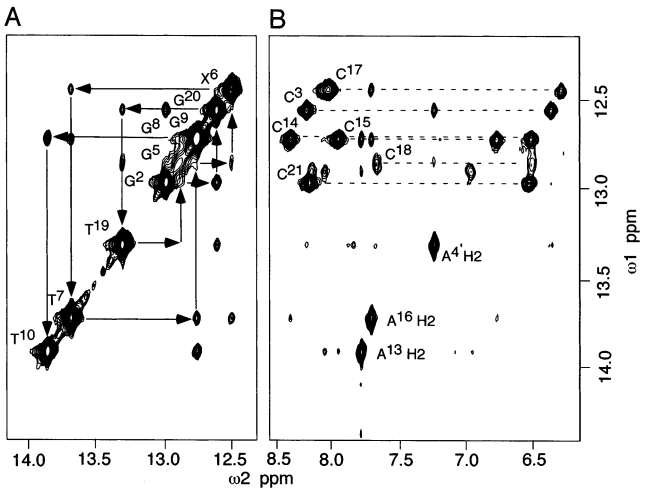

FIGURE 2: (A) Expanded plot showing sequential NOE connectivities for the imino protons of the BA-modified codon 12 oligodeoxynucleotide. The labels represent the imino proton of the designated base. (B) Expanded plot showing cross-peaks between dG imino protons and dC amino protons in G·C base pairs and between dT imino protons and dA H2 protons in A·T base pairs. The 600.13 MHz NOESY spectrum was collected with a mixing time of 250 ms and at 5 °C.

was observed at δ 1.42 ppm. Likewise, for T^{19}, H2′ was observed at δ 1.88 ppm and H2″ was observed at δ 2.24 ppm. The pattern of upfield chemical shifts was also observed for C^{18} H3′, observed at δ 4.08 ppm, and T^{19} H4′, observed at δ 4.2 ppm. The deoxyribose H5′ and H5″ protons were assigned, to the extent possible, on the basis of the expectation that the H5″ resonance was downfield of the H5′ resonance. The chemical shifts of the nonexchangeable protons are listed in Table S1 of the Supporting Information.

Exchangeable Protons. An expanded region showing cross-peaks between the imino protons is given in Figure 2. Assignment of the imino protons was made from NOE connectivities between adjacent base pairs and connectivities to the base-paired amino protons (*73*). Sequential assignments of the imino protons from base pairs G^2·C^{21} → T^{10}·A^{13} were obtained unequivocally. The imino proton resonance from the 5′-neighbor G^5 N1H proton was broadened, suggesting an increased rate of exchange with solvent. The imino resonance arising from the modified nucleotide X^6 N1H proton was observed at δ 12.4 ppm. It showed the expected NOEs to T^7 N3H and A^{16} H2 from the 3′-neighbor T^7·A^{16} base pair. It showed a weak NOE in the 5′-direction, to G^5 N1H of the 5′-neighbor G^5·C^{18} base pair.

With the exception of the 5′-terminal nucleotides G^1 and C^{12}, distinctive amino protons were observed for each cytosine (Figure 2). The non-hydrogen-bonded amino protons of cytosine were assigned from their cross-peaks to the resonances of the hydrogen-bonded amino protons. The amino proton resonances of nucleotide C^{18}, belonging to the 5′-neighbor G^5·C^{18} base pair, were broadened compared to the resonances of the other cytosine amino protons. It was not possible to assign the X^6 amino proton. The chemical shifts of the exchangeable protons are listed in Table S2 of the Supporting Information.

Benz[a]anthracene Protons. An expanded region of the NOESY spectrum used for the assignment of BA aromatic protons is shown in Figure 3. Fifteen BA−BA NOEs were used to assign the aromatic protons of benz[*a*]anthracene, in combination with DQF-COSY and TOCSY data. A DQF-COSY spectrum revealed three cross-peaks, corresponding to ^3J ^{1}H couplings between BA H5 and H6, BA H8 and H9, and BA H10 and H11 protons. The BA H12 resonance was identified by the BA H11−BA H12 NOE. Likewise, the BA H7 resonance showed both BA H7−BA H6 and BA H7−BA H8 NOEs. The BA aromatic proton assignments were verified by a TOCSY experiment. The aliphatic protons of the BA cyclohexene ring were identified from COSY and NOESY data. These resonances were found in the 4−5 ppm spectral region. The chemical shifts of the BA resonances are listed in Table S3 of the Supporting Information.

Benz[a]anthracene−DNA NOEs. NOEs between protons of the BA moiety and the DNA involved deoxyribose protons of nucleotides X^6 and T^7 in the modified strand and nucleotides C^{18} and T^{19} in the complementary strand (Figure 4 and Figure S2 of the Supporting Information). Several of the deoxyribose proton resonances overlapped in the spectrum, but nine NOEs could be uniquely identified. BA H2 exhibited an NOE to T^7 H1′, as did BA H3. These protons were located on the cyclohexenyl ring of BA. Of the aromatic BA protons, BA H6 exhibited an NOE to T^{19} H5′. BA H7 exhibited an NOE to T^{19} H5″ and BA H9 an NOE to T^{19} H4′. BA H10 exhibited a weak NOE to T^{19} H4′. BA H11 also had an NOE to X^6 H1′, and an NOE to T^{19} H4′. BA H12 exhibited an NOE to X^6 H1′. Several additional BA-DNA NOEs were not uniquely assigned due to spectral overlap. BA H5 and H6 exhibited NOEs to an overlapped set of three resonances assigned as C^{18} H4′, H5′, and H5″. BA H6, BA H7, and BA H8 each exhibited NOEs to an

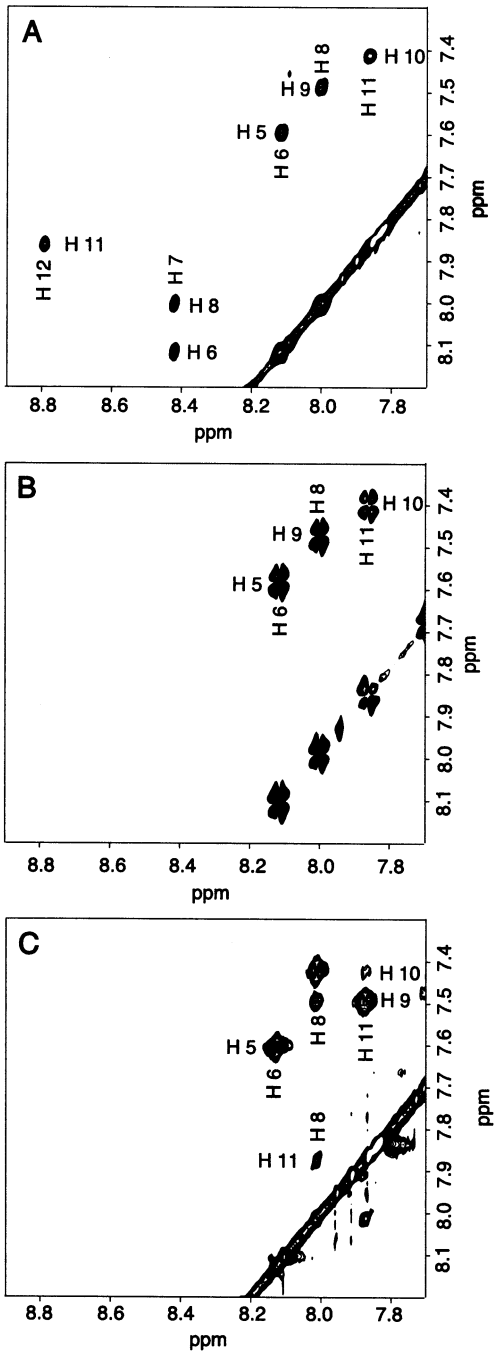

FIGURE 3: Expanded regions of the 800.23 MHz (A) NOESY spectrum with a mixing time of 200 ms, (B) DQF-COSY spectrum, and (C) TOCSY spectrum with a mixing time of 100 ms, used to derive the assignments for the BA aromatic protons. The experiments were carried out at 25 °C.

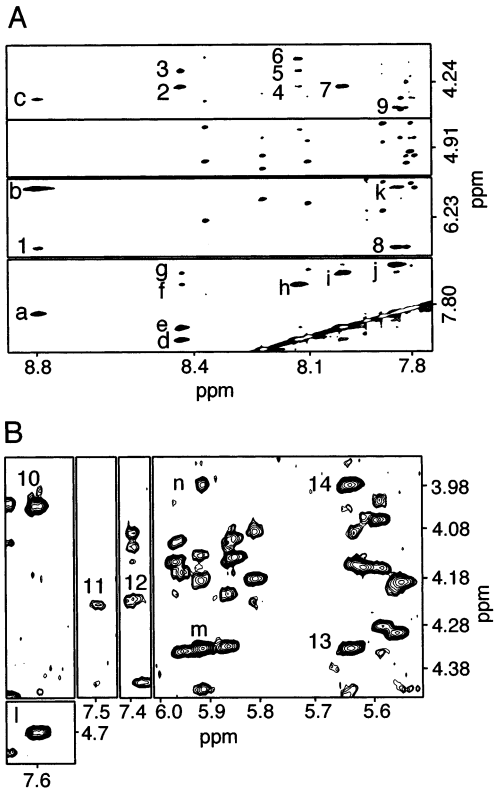

FIGURE 4: Tile plot expansion of a NOESY spectrum showing cross-peaks involving BA protons. The BA−DNA cross-peaks are numbered as follows: (1) BA H12 → X^6 H1′, (2) BA H7 → T^{19} H4′, H5′ (overlap), (3) BA H7 → T^{19} H5″, (4) BA H6 → T^{19} H5′, (5) BA H6 → T^{19} H5″, (6) BA H6 → C^{18} H4′, H5′, H5″ (overlap), (7) BA H8 → T^{19} H4′, H5′ (overlap), (8) BA H11 → X^6 H1′, (9) BA H11 → X^6 H4′, (10) BA H5 → C^{18} H4′, H5′, H5″ (overlap), (11) BA H9 → T^{19} H4′, (12) BA H10 → T^{19} H4′, (13) BA H2 → T^7 H1′, and (14) BA H3 → T^7 H1′. The BA−DNA cross-peaks indicated that BA was in the minor groove and oriented toward the 5′-direction. The BA−BA cross-peaks are as follows: (a) BA H12 → BA H11, (b) BA H12 → BA H1, (c) BA H12 → BA H2, (d) BA H7 → BA H6, (e) BA H7 → BA H8, (f) BA H7 → BA H5, (g) BA H7 → BA H9, (h) BA H6 → BA H5, (i) BA H8 → BA H9, (j) BA H11 → BA H10, (k) BA H11 → BA H1, (l) BA H5 → BA H4, (m) BA H1 → BA H2, and (n) BA H1 → BA H3.

overlapped set of two resonances assigned as T^{19} H4′ and H5′.

Torsion Angle Analysis. Evaluation of the DQF-COSY data suggested that the pseudorotation for C^{17} was shifted into the C1′-*exo* range. It was not possible to extract *J* coupling data for C^{18} and T^{19} due to spectral overlap which occurred as a consequence of the upfield chemical shifts of the H1′, H2′, and H2″ resonances from these nucleotides. With the exception of C^{18} and T^{19}, the remainder of the nucleotides favored the C2′-*endo* sugar ring conformation. It was not possible to determine ^{1}H *J* couplings associated with the cyclohexene ring of the BA moiety due to line broadening. Measurements for the phosphodiester backbone torsion angles ϵ and ζ were obtained from a heteronuclear ^{1}H−^{31}P correlation experiment. The ^{31}P chemical shifts were observed in the expected chemical shift range. With the exception of nucleotides C^{18} and T^{19}, for which data were not obtained, the ^3J ^{1}H−^{31}P couplings for ϵ and ζ were in the expected range for B-DNA.

Chemical Shift Perturbations. The chemical shifts of the nonexchangeable and exchangeable protons, compared to those of the unmodified *ras12* sequence, are shown in Figure 5. These perturbations were localized near the site of adduction. They involved base pairs located in the 5′-direction from X^6. Upfield chemical shifts of 0.25 ppm for C^{18} H6 and 0.2 ppm for T^{19} H6 were observed. A downfield chemical shift of 0.4 ppm was observed for X^6 H8. Significant changes in chemical shift were observed for sugar protons proximate to the adducted nucleotide X^6. A 0.6 ppm downfield shift was detected for X^6 H1′. The sugar protons X^6 H2′ and H2″ experienced downfield shifts of 0.2 ppm. In the complementary strand, C^{18} H1′ shifted 1.6 ppm upfield.

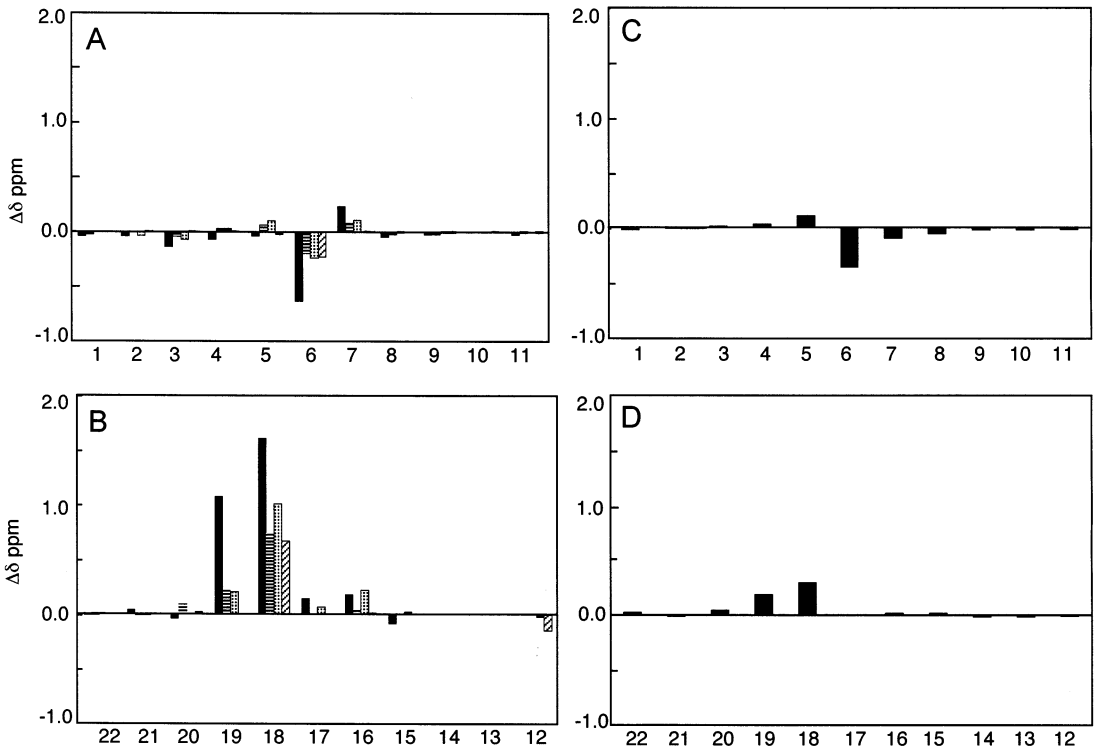

FIGURE 5: Chemical shift changes of selected protons relative to the unmodified oligodeoxynucleotide duplex. (A) Deoxyribose protons in the modified strand. (B) Deoxyribose protons in the complementary strand: (solid bars) H1′, (striped bars) H2′, (spotted bars) H2″, and (cross-hatched bars) H3′. (C) Nucleotide H8 and H6 protons in the modified strand. (D) Nucleotide H8 and H6 protons in the complementary strand. Positive values of $\Delta\delta$ represent upfield chemical shift changes. $\Delta\delta = \delta_{\text{unmodified oligodeoxynucleotide}} - \delta_{\text{modified oligodeoxynucleotide}}$.

C^{18} H2′ and H2″ shifted 0.75 ppm upfield. Likewise, C^{18} H3′ shifted 0.7 ppm upfield. T^{19} H1′ shifted 1.1 ppm upfield, and T^{19} H2′ and H2″ shifted 0.25 ppm upfield. T^{19} H3′ exhibited a 0.25 ppm upfield shift. The upfield shifts for T^{19} deoxyribose protons were significant because the A^4·T^{19} base pair was two bases to the 5′-direction from the site of adduction.

Restrained Molecular Dynamics Calculations

A total of 426 experimental distance restraints were used. These included nine BA−DNA distances that were determined from uniquely assigned BA−DNA NOEs. The DNA distance restraints were approximately evenly distributed along the length of the duplex. A list of the experimental distance restraints along with the upper and lower bounds is shown in Table S4 of the Supporting Information. The torsion angle restraints included 90 sugar pucker restraints. Also, 40 experimentally determined phosphodiester backbone angle restraints were included. These angles were restrained to 165 ± 30° and −105 ± 25°, the exceptions being C^{18} and T^{19}, for which torsion angle restraints were not obtained. The conformation of the BA cyclohexene ring was not defined by torsion angle restraints in the rMD calculations, since it was not possible to extract *J* couplings for these resonances. Empirical base pair planarity restraints were used, except at the modified X^6·C^{17} base pair and at adjacent A^4·T^{19}, G^5·C^{18}, and T^7·A^{16} base pairs. The rationale for inclusion of the planarity restraints was 2-fold (Figure 2). First, a complete set of NOEs was observed between the imino and amino protons of G·C base pairs, and between the imino and H2 protons of A·T base pairs. Second, a complete set of NOEs was observed between imino protons found in adjacent base pairs along the duplex.

Randomly seeded rMD calculations were initiated from both A-form (IniA) and B-form (IniB) starting structures (Figure 6). The maximum pairwise rmsd for the emergent structures arising from either the IniA or IniB starting structure was 0.5 Å. This suggested that the ensemble of structures emerging from the rMD calculations were reasonably converged. The calculated rmsd between the average structure emergent from the rMD calculations and the A-form starting structure was 3.5 Å. The calculated rmsd between the average structure emergent from the rMD calculations and the B-form starting structure was 2.7 Å. The calculated rmsd between the averaged structures initiated from either the B-form or A-form starting structures was 1.40 Å. The structures emergent from the rMD calculations differed from both the A-form and B-form starting structures. However, they more closely approximated B-form DNA. The total energies and NOE restraint violation energies for converged structures were lower than 3 and 0.04 kcal/mol, respectively. None of the reported NOE violations involved NOEs between BA and DNA.

The accuracy of the calculated structures was judged by complete relaxation matrix analysis using CORMA (*52*). The overall sixth-root residual R_1^x, calculated between the theoretical NOE intensities predicted by the refined structure and the actual NOE intensities, was 8.5×10^{-2} (Table 1). Figure 7 shows the distribution of R_1^x values for intranucleotide and internucleotide NOEs, for each base pair in the oligodeoxynucleotide duplex. The residuals were consistently on the order of 10% in both strands of the duplex. The CORMA calculations suggested reasonable agreement between the refined structure and the NOE data. Accuracy was also judged by comparing the distance restraints between BA protons and DNA protons predicted by MARDIGRAS,

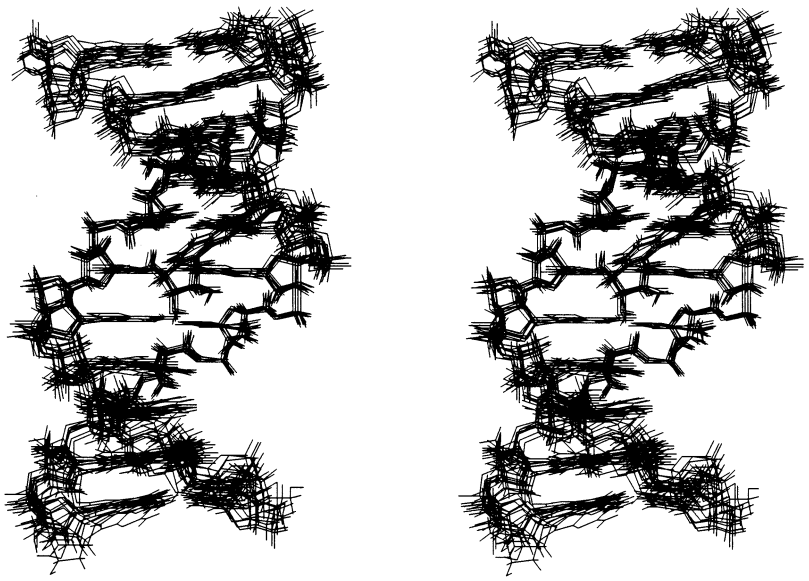

FIGURE 6: Stereoview showing the convergence of an ensemble of 10 rMD structures emergent from rMD calculations initiated with a B-form starting structure ⟨rMDBi⟩.

Table 1: Structural Refinement Statistics for the rMD-Generated Structures of the BA SRSR (12,2) Adduct

no. of experimental restraints	
intranucleotide distance	298
internucleotide distance[a]	127
total distance	426
BA−DNA distance[b]	17
BA−BA distance	15
sugar pucker[c]	90
backbone torsion angle[d]	40
structural statistics	
NMR *R*-factor (R_1^x)[e,f]	
$rMD_{A,avg}$	0.084
$rMD_{B,avg}$	0.089
rms deviation from ideal geometry	
bond lengths (Å)	0.019 ± 0.005
bond angles (deg)	2.139 ± 0.008
pairwise rms deviation over all atoms (Å)[g]	
IniA−IniB	5.99
$\langle rMD_{1A}\rangle$−IniA	3.475 ± 0.244
$\langle rMD_{1B}\rangle$−IniB	2.753 ± 0.235
$\langle rMD_{1B}\rangle$−$\langle rMD_{1B}\rangle$	0.539 ± 0.124
$\langle rMD_{1A}\rangle$−$\langle rMD_{1A}\rangle$	0.526 ± 0.095
$rMD_{A,avg}$ vs $rMD_{B,avg}$	1.4
rms deviation of NOE violations ($\times 10^{-2}$)	5.70 ± 0.02
no. of DNA−DNA NOE violations (>0.1 Å)	19
no. of BA−DNA NOE violations (>0.1 Å)	0
no. of BA−BA NOE violations (>0.1 Å)	2

[a] Does not include empirical base pairing restraints. [b] Nine of the BA−DNA distance restraints were calculated from BA−DNA NOE cross-peaks that were uniquely assigned in the spectrum; the remainder were estimated from BA−DNA NOE cross-peaks that involved spectral overlap. [c] Sugar pucker restraints not obtained for C^{18} and T^{19}. [d] Backbone restraints not obtained for C^{18} and T^{19}. [e] $rMD_{1A,avg}$, $rMD_{1B,avg}$, and $rMD_{2B,avg}$ are the potential energy-minimized average structures from the sets of structures resulting from the first (rMD_1) and second (rMD_2) generation of molecular dynamics calculations. The mixing time used to calculate R_1^x was 200 ms. [f] $R_1^x = \sum|(a_o)_i^{1/6} - (a_c)_i^{1/6}|/\sum|(a_o)_i^{1/6}|$, where a_o and a_c are the intensities of observed (non-zero) and calculated NOE cross-peaks, respectively. [g] The broken brackets represent the group of structures.

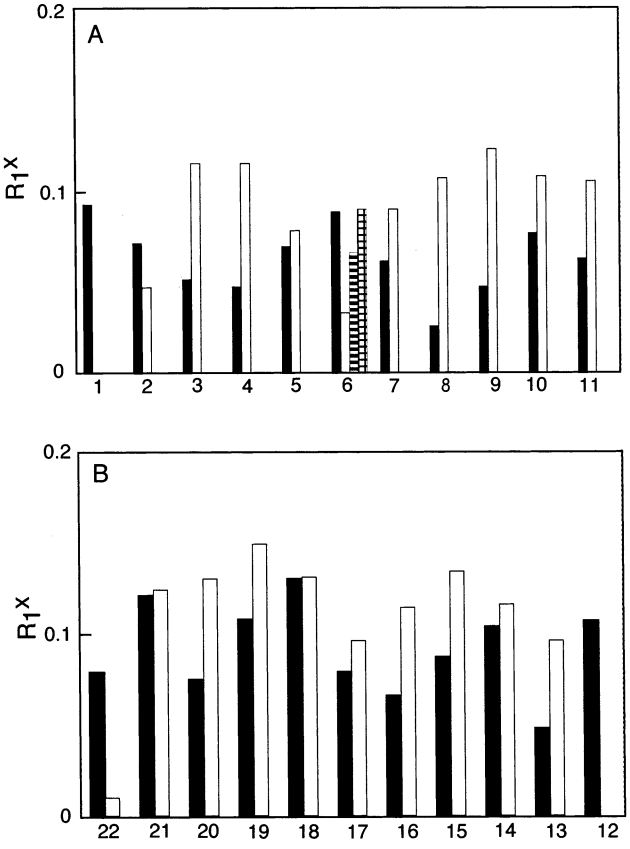

FIGURE 7: Bar diagrams showing the per-residue residual R_1^x values resulting from a comparison of theoretical NOE intensities calculated using CORMA for the refined structures, with the experimental NOE intensities of the BA SRSR (12,2) adduct. (A) Modified strand. (B) Complementary strand. The filled bars show the intraresidue R_1^x values. The empty bars show the inter-residue R_1^x values. The cross-hatched bar shows the interstrand R_1^x values between X^6 and C^{18}, and the checkered bar shows the interstrand R_1^x values between X^6 and T^{19}.

with the actual distances predicted by the rMD calculations. The calculated BA−DNA distances observed in the refined structure were within ±20% of the corresponding distance restraint values used in the rMD calculations.

Structure of the Adduct

The structure that emerged from the rMD calculations was a right-handed duplex, in which the BA moiety was in the

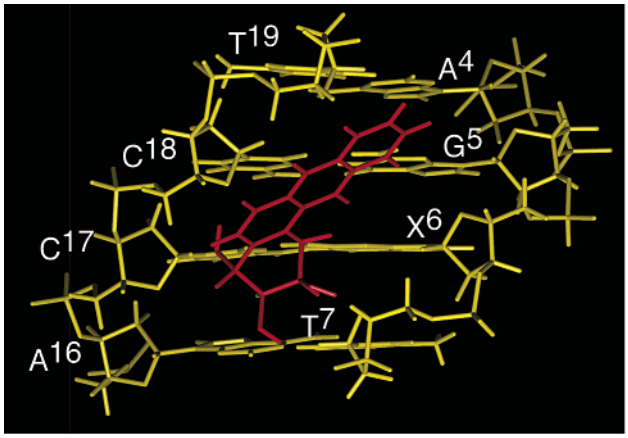

FIGURE 8: Side view of the d($A^4G^5X^6T^7$)·d($T^{19}C^{18}C^{17}A^{16}$) segment of the BA SRSR (12,2) adduct from the minor groove. The BA moiety is in red and is extended in the direction of the A^4·T^{19} base pair.

minor groove, shown in Figure 8. It was oriented in the 5′-direction from nucleotide X^6. The BA moiety extended almost two base pairs in the 5′-direction toward the A^4·T^{19} base pair. Accommodation of the BA aromatic rings in the minor groove allowed for maintenance of Watson−Crick type base pairing adjacent to the lesion site. Helicoidal analysis suggested the width of the minor groove at the site of adduction, and extending in the 5′-direction, was 13 ± 0.5 Å. The values for helical twist and base pair rise at the adducted site remained within the range anticipated for a B-like duplex, consistent with the conclusion that the BA moiety was accommodated within the minor groove. The calculations predicted that the BA aromatic rings were proximate to deoxyribose sugars at nucleotides C^{17}, C^{18}, and T^{19} in the complementary strand. The BA moiety was oriented such that BA protons H5−H8 faced toward the complementary strand. Protons H9 and H10 faced in the 5′-direction toward the A^4·T^{19} base pair. The calculations predicted that these protons should show NOEs to deoxyribose protons of T^{19}, but not to the minor groove proton A^4 H2. Protons H11 and H12 were in the minor groove and faced the modified strand of the duplex.

DISCUSSION

The site-specific adduction of DNA by stereoisomeric PAH diol epoxides is generally believed to represent the means by which chemicals in this class of mutagens initiate their genotoxic effects. Adducts at guanine N^2 generally represent the predominant chemically stable adducts for PAH diol epoxides. Consequently, considerable effort has been spent to elucidate solution structures of the stereoisomeric bay region PAH−N^2-dG adducts (*28*, *37*). In general, the conformations of guanine N^2 adducts of bay region PAH depend on the stereochemistry of the cyclohexene ring, particularly at the benzylic carbon, and also on DNA sequence (*28*).

Structure of the BA SRSR (12,2) Adduct. Several lines of evidence supported the conclusion that the BA aligned in the minor groove in the 5′-direction with respect to the modified nucleotide X^6, as predicted by the rMD calculations. These included the pattern of chemical shift perturbations which involved the X^6·C^{17} lesion site, and extended in the 5′-direction, involving nucleotides C^{18} and T^{19} in the complementary strand (Figure 5). Also, the pattern of NOEs observed between the BA protons and the DNA extended in the 5′-direction from the adducted site, also primarily involving the adducted X^6·C^{17} base pair, and nucleotides C^{18} and T^{19} in the complementary strand. There was no interruption in sequential NOE connectivities between base and deoxyribose H1′ resonances, either for the aromatic and anomeric region or for the imino regions of the spectra. Watson−Crick type hydrogen bonding was maintained at the X^6·C^{17} base pair, as evidenced by observation of the N1 imino proton resonance and NOEs between the imino resonance and the amino protons of nucleotide C^{17} (Figure 2). The predicted orientation of the BA aromatic protons H5−H9 toward the unmodified strand was consistent with NOEs observed to deoxyribose protons of C^{18} and T^{19} (Figure 4). Although the BA moiety extended in the 5′-direction toward the A^4·T^{19} base pair, the rMD calculations predicted that the BA H9 and H10 protons were not within 5 Å of the minor groove A^4 H2 proton. This was consistent with the failure to observe NOEs between BA H9 and H10 and A^4 H2. The NOEs between BA H1, H11, and H12 and X^6 H1′ were explained by the predicted location of these protons facing X^6. The line broadening of the Watson−Crick hydrogen-bonded imino resonance and the C^{18} NH_2 resonances at the G^5·C^{18} base pair suggested a thermal destabilization of this base pair, accompanied by an increased level of proton exchange, in the presence of the BA lesion.

Molecular Topology. In Chart 2, the topology of the BA SRSR (12,2) adduct is compared with that of the corresponding BP, 5MC, and BcPh adducts having comparable stereochemistry. The (+)-*trans-anti*-[BP]−N^2-dG adduct oriented in the minor groove in the 5′-direction (*29*, *30*) in a manner similar to that of the presently examined BA SRSR (12,2) adduct. However, the BA ring system extended further in the 5′-direction in the groove than did the BP ring system (*29*, *30*). The rMD calculations suggested that the BA moiety extended in the 5′-direction toward the A^4·T^{19} base pair, two base pairs in the 5′-direction from X^6 (Figure 8). The topology of the BA aromatic rings as compared to the BP aromatic rings suggested that BA, when embedded in the minor groove, was more shielded from solvent than was BP. In contrast to BA and BP, the (−)-*trans-anti*-[BcPh]−N^2-dG adduct, which possessed the fjord region ring, intercalated in the 5′-direction at the adducted site (*37*). The (+)-*trans-anti*-[5MC]−N^2-dG adduct with the corresponding stereochemistry (4*S* at the benzylic carbon) was disordered and did not yield a refined solution structure (*28*). It provided an interesting contrast in that the methyl group was at the fjord position. Its topology may simultaneously hinder minor groove binding, as observed for the (+)-*trans-anti*-[BP]−N^2-dG (*29*, *30*) and *trans-anti*-[BA]−N^2-dG adducts, and intercalation, as observed for the (−)-*trans-anti*-[BcPh]−N^2-dG adduct (*37*).

PAH topology modulates conformation differently for adducts at guanine N^2 versus adducts at adenine N^6. Both the *trans-anti*-[BP]−N^2-dG and *trans-anti*-[BA]−N^2-dG adducts exhibited minor groove binding, oriented in the 5′-direction. This was not the case for the corresponding adenine N^6 adducts of these two PAH lesions. When adducted to adenine N^6, both exhibited multiple conformations in duplex DNA, indicating some degree of structural disorder at the lesion sites. Two conformations in slow exchange on the

Chart 2: Comparative Topology of *trans-anti*-[BA]−N^2-dG, 10*S*-(+)-*trans-anti*-[BP]−N^2-dG, 4*S*-(+)-*trans-anti*-[5MC]−N^2-dG, and 1*S*-(−)-*trans-anti*-[BcPh]−N^2-dG Adducts[a]

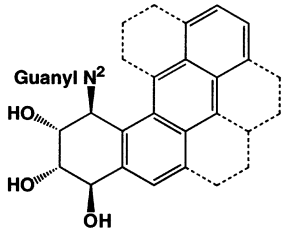

1*S*-*trans-anti*-[BA]-N²-dG Adduct

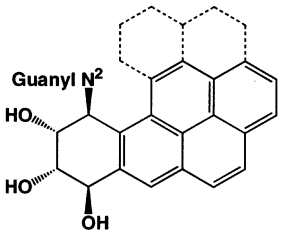

10*S* (+)-*trans-anti*-[BP]-N²-dG Adduct

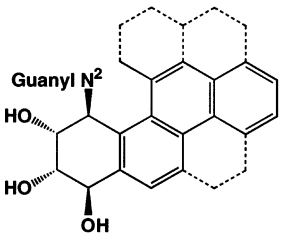

4*S* (+)-*trans-anti*-[5MC]-N²-dG Adduct

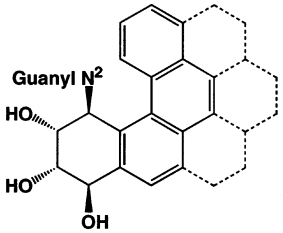

1*S* (-)-*trans-anti*-[BcPh]-N²-dG Adduct

[a] In each instance, the stereochemical assignment proceeding counterclockwise from the benzylic carbon of the cyclohexenyl ring is *S,R,S,R.* Dotted lines in each instance represent overlays of aromatic rings present in one or more of the other three topologies.

NMR time scale existed for the *trans-anti*-[BA]−N^6-dA adduct. In the major conformation, an *anti* glycosidic torsion angle was observed for the adducted dA. The refined structure was a right-handed duplex, with the BA moiety intercalated on the 3′-face of the modified base pair, from the major groove (*74*). Multiple conformations also existed for the corresponding *trans-anti*-[BP]−N^6-dA adduct. In the major conformation, the modified dA was rotated about the glycosyl bond into the *syn* conformation, to enable 3′-intercalation of the aromatic ring system moiety (*75*). Thus, the topology that facilitated minor groove binding at guanine N^2 resulted in 3′-intercalation accompanied by structural disorder at adenine N^6. Yet another pattern emerged with benzo[*c*]phenanthrene adducts having *S* stereochemistry at the benzylic carbon. These intercalated when adducted to either guanine N^2 (*37*) or adenine N^6 (*76*, *77*). Overall, the various results suggest that a complex interplay between multiple factors, including stereochemistry and sequence, in combination with topology, modulates PAH adduct structure in duplex DNA.

Biological Implications. The conformational diversity of PAH adducts in DNA is anticipated to play a role in their subsequent biological processing (*78*). Excision of site-specific *trans-anti*-[PAH]−N^2-dG adducts by the human nucleotide excision repair system correlated with minor groove conformations versus intercalative conformations (*79*, *80*). Lin et al. (*37*) argued that the molecular topology of PAH adducts modulated repair. The minor groove (+)-*trans-anti*-[BP]−N^2-dG lesion was a better substrate for nucleotide excision repair than was the intercalated (−)-*trans-anti*-[BcPh]−N^2-dG lesion. It was proposed that intercalated fjord region PAH adducts were less efficiently recognized by the nucleotide excision repair apparatus than the minor groove-bound nonfjord region PAH (*81*). Our results suggest the *trans-anti*-[BA]−N^2-dG adduct in duplex DNA more closely resembles the (+)-*trans-anti*-[BP]−N^2-dG adduct and not the (−)-*trans-anti*-[BcPh]−N^2-dG adduct. It will be of interest to determine if this structural correlation with the (+)-*trans-anti*-[BP]−N^2-dG adduct is reflected in the recognition of the *trans-anti*-[BA]−N^2-dG adduct by the nucleotide excision repair apparatus.

DNA Sequence Considerations. These studies were conducted at 25 °C. A single set of resonances was observed in the ^{1}H spectrum, consistent with a single conformation of the BA SRSR (12,2) adduct. At 5 °C, additional ^{1}H resonances were observed. These were not assigned. However, they were consistent with the spectral line broadening for the G^5•C^{18} base pair observed at 25 °C, and suggested formation of a less stable minor conformation of the BA SRSR (12,2) adduct at lower temperatures. This was consistent with observations that T•A base pairs flanking guanine N^2 PAH lesions induced greater disorder to duplex DNA. For example, when the (+)-*trans-anti*-[BP]−N^2-dG lesion was placed into the 5′-TXC-3′ sequence, Fountain and Krugh (*35*) reported exchange broadening in the ^{1}H spectrum, suggesting the presence of a second minor conformation.

ACKNOWLEDGMENT

We thank Mr. Markus Voehler for assistance with the collection of NMR data.

SUPPORTING INFORMATION AVAILABLE

Chemical shift assignments for the base and deoxyribose protons of the BA SRSR (12,2) duplex (Table S1), chemical shift assignments for the imino and amino protons of the BA SRSR (12,2) duplex (Table S2), chemical shift assignments for the BA protons of the BA SRSR (12,2) duplex (Table S3), distance restraints used for rMD calculations of the BA SRSR (12,2) duplex (Table S4), and partial charges used for rMD calculations of the BA SRSR (12,2) duplex

(Figure S1). This material is available free of charge via the Internet at http://pubs.acs.org.

REFERENCES

1. Grimmer, G. (1979) in *Environmental Carcinogens: Selected Methods of Analysis III*, International Agency for Research on Cancer, Lyon, France.
2. International Agency for Research on Cancer (1983) in *Evaluation of Carcinogenic Risk of the Chemical to Man: Certain Polycyclic Aromatic Hydrocarbons and Heterocyclic Compounds*, International Agency for Research on Cancer, Lyon, France.
3. Snook, M. E., Severson, R. F., Arrendale, R. F., Higman, H. C., and Chortyk, O. (1977) *Beitr. Tabakforsch. 9*, 79−101.
4. Yang, S. K. (1988) *Biochem. Pharmacol. 37*, 61−70.
5. Guengerich, F. P., Kim, D. H., and Iwasaki, M. (1991) *Chem. Res. Toxicol. 4*, 168−176.
6. Thakker, D. R., Levin, W., Yagi, H., Tada, M., Ryan, D. E., Thomas, P. E., Conney, A. H., and Jerina, D. M. (1982) *J. Biol. Chem. 257*, 5103−5110.
7. Wood, A. W., Chang, R. L., Levin, W., Lehr, R. E., Schaefer-Ridder, M., Karle, J. M., Jerina, D. M., and Conney, A. H. (1977) *Proc. Natl. Acad. Sci. U.S.A. 74*, 2746−2750.
8. Slaga, T. J., Huberman, E., Selkirk, J. K., Harvey, R. G., and Bracken, W. M. (1978) *Cancer Res. 38*, 1699−1704.
9. Wood, A. W., Levin, W., Chang, R. L., Lehr, R. E., Schaefer-Ridder, M., Karle, J. M., Jerina, D. M., and Conney, A. H. (1977) *Proc. Natl. Acad. Sci. U.S.A. 74*, 176−179.
10. Cooper, C. S., Ribeiro, O., Farmer, P. B., Hewer, A., Walsh, C., Pal, K., Grover, P. L., and Sims, P. (1980) *Chem.-Biol. Interact. 32*, 209−231.
11. Cary, P. D., Turner, C. H., Cooper, C. S., Ribeiro, O., Grover, P. L., and Sims, P. (1980) *Carcinogenesis 1*, 505−512.
12. Wood, A. W., Chang, R. L., Levin, W., Thakker, D. R., Yagi, H., Sayer, J. M., Jerina, D. M., and Coney, A. H. (1984) *Cancer Res. 44*, 2320−2324.
13. Wood, A. W., Levin, W., Lu, A. Y., Ryan, D., West, S. B., Lehr, R. E., Schaefer-Ridder, M., Jerina, D. M., and Conney, A. H. (1976) *Biochem. Biophys. Res. Commun. 72*, 680−686.
14. Dipple, A., Moschel, R. C., and Bigger, C. A. H. (1984) in *Chemical Carcinogens* (Searle, C. E., Ed.) pp 41−163, American Chemical Society, Washington, DC.
15. Thakker, D. R., Levin, W., Yagi, H., Ryan, D., Thomas, P. E., Karle, J. M., Lehr, R. E., Jerina, D. M., and Conney, A. H. (1979) *Mol. Pharmacol. 15*, 138−153.
16. Thakker, D. R., Yagi, H., Levin, W., Wood, A. W., Conney, A. H., and Jerina, D. M. (1985) in *Bioactivation of Foreign Compounds* (Anders, M. W., Ed.) pp 177−242, Academic Press, New York.
17. Jennette, K. W., Jeffery, A. M., Blobstein, S. H., Beland, F. A., Harvey, R. G., and Weinstein, I. B. (1977) *Biochemistry 16*, 932−938.
18. Osborne, M. R. (1990) *Chem.-Biol. Interact. 75*, 131−140.
19. Osborne, M. R., Jacobs, S., Harvey, R. G., and Brookes, P. (1981) *Carcinogenesis 2*, 553−558.
20. Jeffery, A. M., Jennette, K. W., Blobstein, S. H., Weinstein, I. B., Beland, F. A., Harvey, R. G., Kasai, H., Miura, I., and Nakanishi, K. (1976) *J. Am. Chem. Soc. 98*, 5714−5715.
21. Cheng, S. C., Hilton, B. D., Roman, J. M., and Dipple, A. (1989) *Chem. Res. Toxicol. 2*, 334−340.
22. Cosman, M., Ibanez, V., Geacintov, N. E., and Harvey, R. G. (1990) *Carcinogenesis 11*, 1667−1672.
23. Mao, B., Margulis, L. A., Li, B., Ibanez, V., Lee, H., Harvey, R. G., and Geacintov, N. E. (1992) *Chem. Res. Toxicol. 5*, 773−778.
24. Margulis, L. A., Ibanez, V., and Geacintov, N. E. (1993) *Chem. Res. Toxicol. 6*, 59−63.
25. Mao, B., Xu, J., Li, B., Margulis, L. A., Smirnov, S., Ya, N.-Q., Courtney, S. H., and Geacintov, N. E. (1995) *Carcinogenesis 16*, 357−365.
26. DeCorte, B. L., Tsarouhtsis, D., Kuchimanchi, S., Cooper, M. D., Horton, P., Harris, C. M., and Harris, T. M. (1996) *Chem. Res. Toxicol. 9*, 630−637.
27. Johnson, F., Bonala, R., Tawde, D., Torres, M. C., and Iden, C. R. (2002) *Chem. Res. Toxicol. 15*, 1489−1494.
28. Geacintov, N. E., Cosman, M., Hingerty, B. E., Amin, S., Broyde, S., and Patel, D. J. (1997) *Chem. Res. Toxicol. 10*, 111−146.
29. Cosman, M., De Los Santos, C., Fiala, R., Hingerty, B. E., Singh, S. B., Ibanez, V., Margulis, L. A., Live, D., Geacintov, N. E., Broyde, S., and Patel, D. J. (1992) *Proc. Natl. Acad. Sci. U.S.A. 89*, 1914−1918.
30. De Los Santos, C., Cosman, M., Hingerty, B. E., Ibanez, V., Margulis, L. A., Geacintov, N. E., Broyde, S., and Patel, D. J. (1992) *Biochemistry 31*, 5245−5252.
31. Cosman, M., De Los Santos, C., Fiala, R., Hingerty, B. E., Ibanez, V., Luna, E., Harvey, R., Geacintov, N. E., Broyde, S., and Patel, D. J. (1993) *Biochemistry 32*, 4145−4155.
32. Cosman, M., Fiala, R., Hingerty, B. E., Amin, S., Geacintov, N. E., Broyde, S., and Patel, D. J. (1994) *Biochemistry 33*, 11518−11527.
33. Cosman, M., Fiala, R., Hingerty, B. E., Amin, S., Geacintov, N. E., Broyde, S., and Patel, D. J. (1994) *Biochemistry 33*, 11507−11517.
34. Cosman, M., Hingerty, B., Geacintov, N. E., Broyde, S., and Patel, D. J. (1995) *Biochemistry 34*, 15334−15350.
35. Fountain, M. A., and Krugh, T. R. (1995) *Biochemistry 34*, 3152−3161.
36. Cosman, M., Xu, R., Hingerty, B. E., Amin, S., Harvey, R. G., Geacintov, N. E., Broyde, S., and Patel, D. J. (1995) *Biochemistry 34*, 6247−6260.
37. Lin, C. H., Huang, X., Kolbanovskii, A., Hingerty, B. E., Amin, S., Broyde, S., Geacintov, N. E., and Patel, D. J. (2001) *J. Mol. Biol. 306*, 1059−1080.
38. Cosman, M., Hingerty, B. E., Luneva, N., Amin, S., Geacintov, N. E., and Broyde, S. (1996) *Biochemistry 35*, 9850−9863.
39. Zegar, I. S., and Stone, M. P. (1996) *Chem. Res. Toxicol. 9*, 114−125.
40. Barbacid, M. (1987) *Annu. Rev. Biochem. 56*, 779−827.
41. Vousden, K. H., Bos, J. L., Marshall, C. J., and Phillips, D. H. (1986) *Proc. Natl. Acad. Sci. U.S.A. 83*, 1222−1226.
42. Setayesh, F. R., DeCorte, B. L., Horton, P., Harris, C. M., Harris, T. M., and Stone, M. P. (1998) *Chem. Res. Toxicol. 11*, 766−777.
43. Zegar, I. S., Setayesh, F. R., DeCorte, B. L., Harris, C. M., Harris, T. M., and Stone, M. P. (1996) *Biochemistry 35*, 4334−4348.
44. Cooper, M. D., Hodge, R. P., Tamura, P. J., Wilkinson, A. S., Harris, C. M., and Harris, T. M. (2000) *Tetrahedron Lett. 41*, 3555−3558.
45. Piotto, M., Saudek, V., and Sklenar, V. (1992) *J. Biomol. NMR 2*, 661−665.
46. Bax, A., Sklenar, V., Clore, G. M., and Gronenborn, A. M. (1987) *J. Am. Chem. Soc. 109*, 6511−6513.
47. Sklenar, V., and Bax, A. (1987) *J. Magn. Reson. 74*, 469−479.
48. Bax, A., and Davis, D. G. (1985) *J. Magn. Reson. 65*, 355−360.
49. Bax, A., and Davis, D. G. (1985) *J. Magn. Reson. 63*, 207−213.
50. Bax, A., Davis, D. G., and Sarkar, S. K. (1985) *J. Magn. Reson. 63*, 230−234.
51. Arnott, S., and Hukins, D. W. L. (1972) *Biochem. Biophys. Res. Commun. 47*, 1504−1509.
52. Keepers, J. W., and James, T. L. (1984) *J. Magn. Reson. 57*, 404−426.
53. Borgias, B. A., and James, T. L. (1990) *J. Magn. Reson. 87*, 475−487.
54. Liu, H., Tonelli, M., and James, T. L. (1996) *J. Magn. Reson., Ser. B 111*, 85−89.
55. Liu, H., Spielmann, H. P., Ulyanov, N. B., Wemmer, D. E., and James, T. L. (1995) *J. Biomol. NMR 6*, 390−402.
56. Schmitz, U., and James, T. L. (1995) *Methods Enzymol. 261*, 3−44.
57. Rinkel, L. J., and Altona, C. (1987) *J. Biomol. Struct. Dyn. 4*, 621−649.
58. Wang, H., Zuiderweg, E. R. P., and Glick, G. D. (1995) *J. Am. Chem. Soc. 117*, 2981−2991.
59. Geen, H., and Freeman, R. (1991) *J. Magn. Reson. 93*, 93−141.
60. Lankhorst, P. P., Haasnoot, C. A. G., Erkelens, C., and Altona, C. (1984) *J. Biomol. Struct. Dyn. 1*, 1387−1405.
61. Gorenstein, D. G. (1992) *Methods Enzymol. 211*, 254−286.
62. Brunger, A. T. (1992) in *X-Plor. Version 3.1. A system for X-ray Crystallography and NMR*, Yale University Press, New Haven, CT.
63. Brooks, B. R., Bruccoleri, R. E., Olafson, B. D., States, D. J., Swaminathan, S., and Karplus, M. (1983) *J. Comput. Chem. 4*, 187−217.
64. Allain, F. H., and Varani, G. (1997) *J. Mol. Biol. 267*, 338−351.
65. Nilsson, L., Clore, G. M., Gronenborn, A. M., Brunger, A. T., and Karplus, M. (1986) *J. Mol. Biol. 188*, 455−475.
66. Clore, G. M., Oschkinat, H., McLaughlin, L. W., Benseler, F., Happ, C. S., Happ, E., and Gronenborn, A. M. (1988) *Biochemistry 27*, 4185−4197.

67. Clore, G. M., Gronenborn, A. M., Carlson, G., and Meyer, E. F. (1986) *J. Mol. Biol. 190*, 259−267.
68. Ryckaert, J.-P., Ciccotti, G., and Berendsen, H. J. C. (1977) *J. Comput. Phys. 23*, 327−341.
69. Lu, X. J., Shakked, Z., and Olson, W. K. (2000) *J. Mol. Biol. 300*, 819−840.
70. Reid, B. R. (1987) *Q. Rev. Biophys. 20*, 2−28.
71. Patel, D. J., Shapiro, L., and Hare, D. (1987) *Q. Rev. Biophys. 20*, 35−112.
72. Chou, S. H., Zhu, L., Gao, Z., Cheng, J. W., and Reid, B. R. (1996) *J. Mol. Biol. 264*, 981−1001.
73. Boelens, R., Scheek, R. M., Dijkstra, K., and Kaptein, R. (1985) *J. Magn. Reson. 62*, 378−386.
74. Li, Z., Kim, H. Y., Tamura, P. J., Harris, C. M., Harris, T. M., and Stone, M. P. (1999) *Biochemistry 38*, 16045−16057.
75. Pradhan, P., Tirumala, S., Liu, X., Sayer, J. M., Jerina, D. M., and Yeh, H. J. (2001) *Biochemistry 40*, 5870−5881.
76. Cosman, M., Fiala, R., Hingerty, B. E., Laryea, A., Lee, H., Harvey, R. G., Amin, S., Geacintov, N. E., Broyde, S., and Patel, D. (1993) *Biochemistry 32*, 2488−2497.
77. Cosman, M., Laryea, A., Fiala, R., Hingerty, B. E., Amin, S., Geacintov, N. E., Broyde, S., and Patel, D. J. (1995) *Biochemistry 34*, 1295−1307.
78. Kozack, R., Seo, K. Y., Jelinsky, S. A., and Loechler, E. L. (2000) *Mutat. Res. 450*, 41−59.
79. Hess, M. T., Gunz, D., Luneva, N., Geacintov, N. E., and Naegeli, H. (1997) *Mol. Cell. Biol. 17*, 7069−7076.
80. Buterin, T., Hess, M. T., Luneva, N., Geacintov, N. E., Amin, S., Kroth, H., Seidel, A., and Naegeli, H. (2000) *Cancer Res. 60*, 1849−1856.
81. Yan, S., Shapiro, R., Geacintov, N. E., and Broyde, S. (2001) *J. Am. Chem. Soc. 123*, 7054−7066.

BI020462K